SUPPLEMENTARY INFORMATION

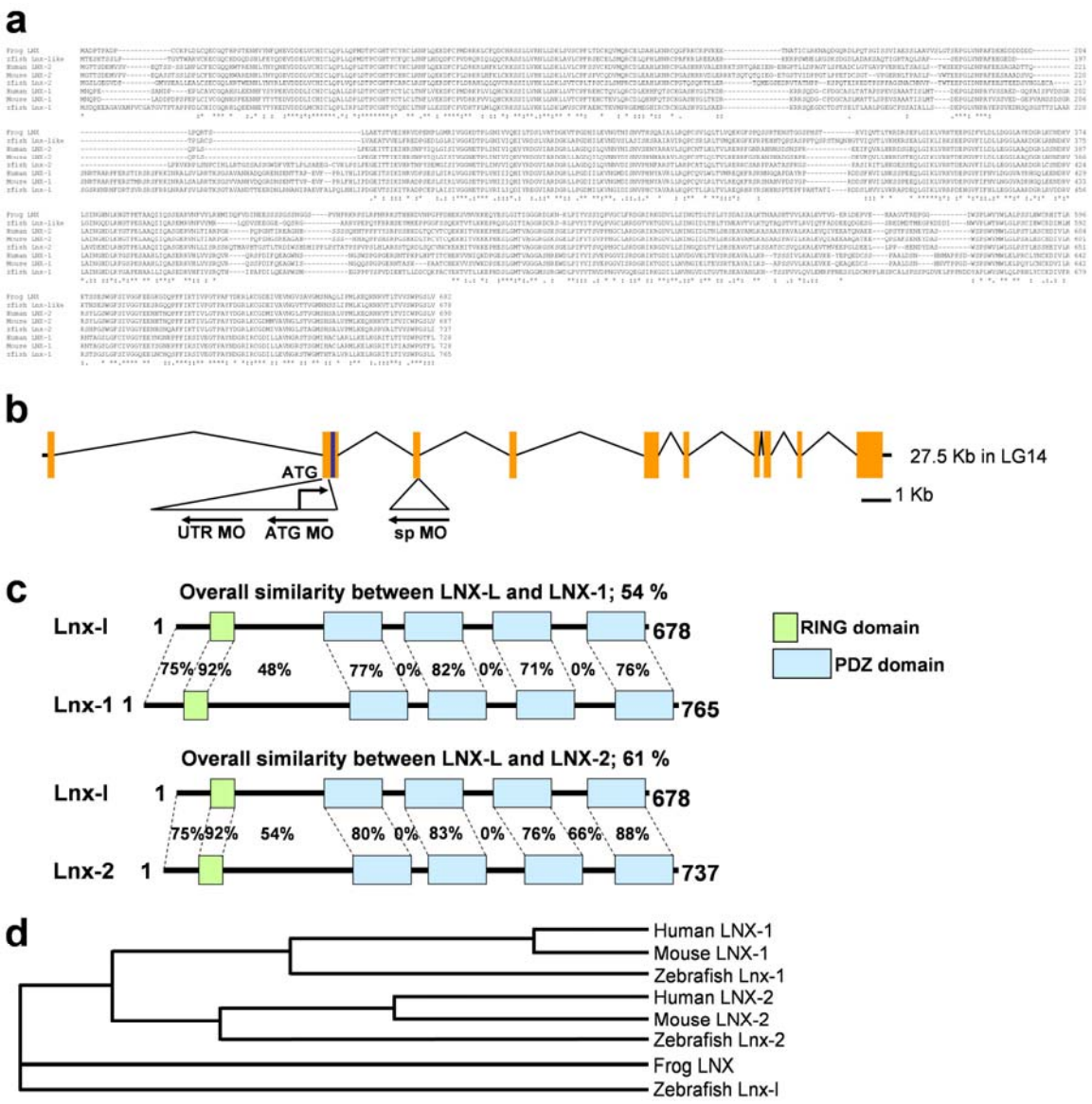

Supplementary Figure 1 | Zebrafish Lnx proteins. We isolated a 3 kb cDNA encoding an unreported member of the LNX family. Since two LNX proteins have been reported in mammals (LNX-1 and LNX-2)[5], we searched for additional zebrafish homologues using BLAST searches and Rapid Amplification of cDNA Ends (RACE) experiments, revealing zebrafish orthologues of mammalian LNX-1 and LNX-2 (Supplementary Figs. 1 and 2). Our original clone is more distantly related to mammalian LNX-1 and LNX-2, and therefore we named it Lnx-like. **a,** Multiple alignment of vertebrate LNX proteins. Alignments were carried out using the ClustalW multiple algorithms. The GenBank

Accession Numbers are: human LNX-1 (BC022983), human LNX-2 (BC036755), mouse Lnx-1 (AF034745), mouse Lnx-2 (AF401681), *Xenopus tropicalis* Lnx (CT025385), zebrafish Lnx-1 (BC124171), zebrafish Lnx-2 (FJ156085) and zebrafish Lnx-l (FJ156084) proteins. **b,** The *lnx-l* gene is composed of ten exons localized on linkage group 14 (LG14). The RING domain of Lnx-l is located in second exon (blue bar). The MO targeting sites are indicated by reverse arrows. ATG stands for the translation start codon. The splicing MO was designed to target the donor site of the third exon. **c.** Lnx proteins including Lnx-l are composed of a RING domain at the N-terminus followed by four PDZ domains. **d.** A phylogenetic tree of vertebrate LNX proteins constructed with TREEVIEW indicates that Lnx-like is not an orthologue of mammalian LNX-1 or LNX-2 but represents a novel member of the

family.

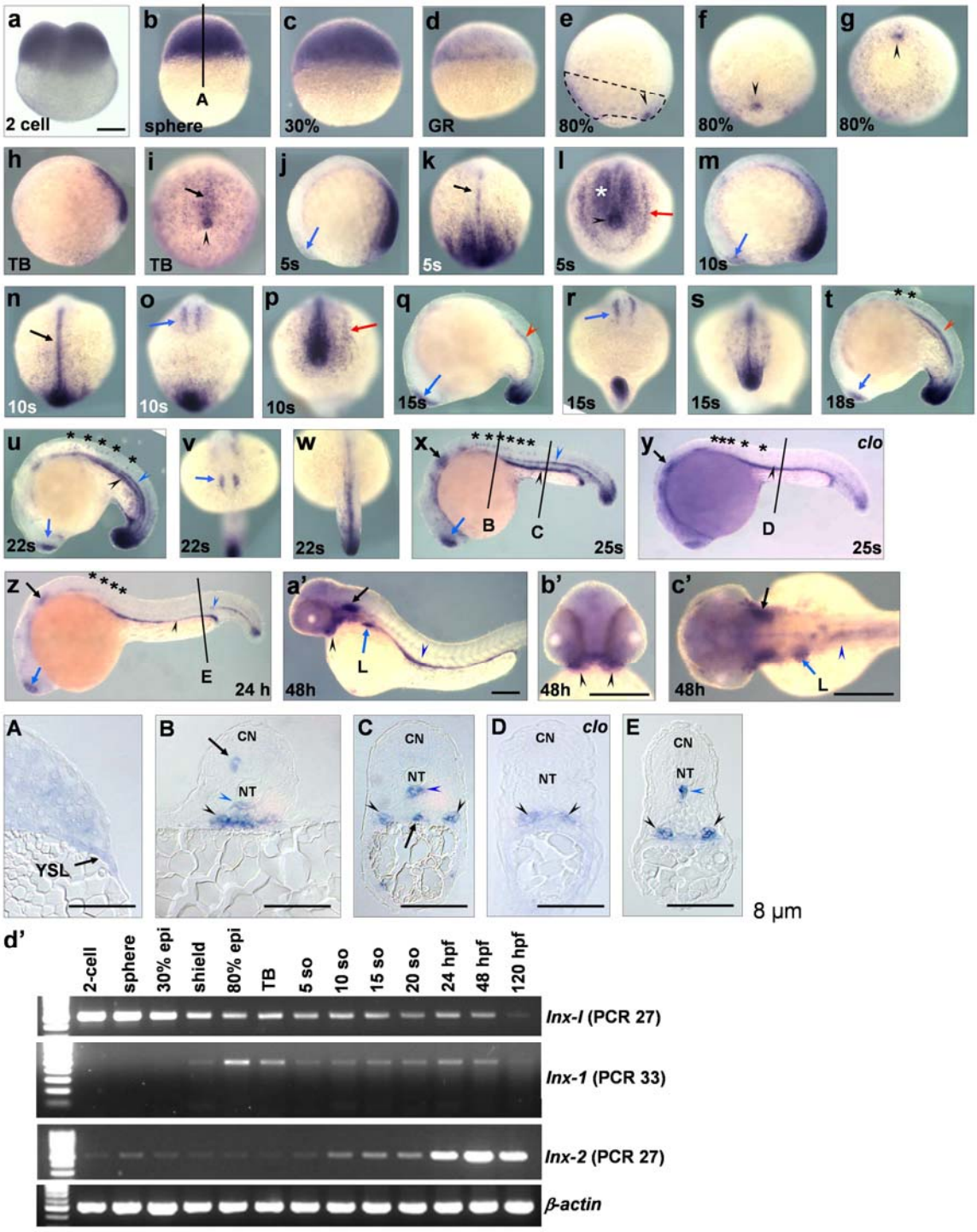

Supplementary Figure 2 | Expression pattern of Lnx-l. a-c, *Lnx-l* is expressed maternally and ubiquitously. **d,** Zygotic expression starts at early gastrulation. **e-g,** 80% epiboly stage. *Lnx-l* shows a gradient ventral-to-dorsal, and is intensely expressed in

dorsal forerunner cells (arrowhead). **e,** Dotted line demarcates expression domain of *lnx-l*. Lateral view. **f,** Dorsal view. **g,** Vegetal view. **h, i,** Tail bud stage; *lnx-l* is expressed in Kupffer's vesicle (arrowhead) and notochord (arrow). **h,** Lateral view. **i,** Posterior view. **j, k,** 5-somite stage. **j,** expression initiates in brain (arrow). Lateral view. **k,** Arrow indicates notochord. Dorsal view. **l,** expression in lateral plate mesoderm (arrow) and presomitic mesoderm (asterisk); arrowhead indicates Kupffer's vesicle. Posterior view. **m-p,** 10-somite stage. **m,** Arrow indicates *lnx-l* transcripts in brain. Lateral view. **n,** Arrow indicates notochord expression of *lnx-l*. Dorsal view, anterior is up. **o,** Arrow shows brain expression of *lnx-l*. Ventral view. **p,** *lnx-l* expression in the lateral plate mesoderm is maintained until the 10-somite stage (arrow). Posterior view. **q-s,** 15-somite stage. **q,** Brain expression (arrow); midline expression in presumptive endothelial tissue (arrowhead). Lateral view. **r,** Brain expression (arrow). Ventral view. **s,** posterior view. **t,** 18-somite stage. Arrow indicates brain. Subset of neuronal cells express *lnx-l* (asterisks). Arrowhead indicates endothelial tissue. Lateral view. **u-w,** 22-somite stage. **u,** Brain (arrow), isolated neuronal cells (asterisks); dorsal aorta (blue arrowhead); pronephric duct (black arrowhead). Lateral view. **v,** Brain (arrow). Anterior view. **w,** Dorsal view. **x,** 25-somite stage. Black arrow indicates otic vesicle, blue arrow the brain; neuronal cells (asterisks); blue arrowhead indicates dorsal aorta; black arrowhead, pronephric duct. Lateral view. **y,** In *cloche*, a mutant lacking endothelium, *lnx-l* expression in the dorsal aorta is abolished, but is maintained in other tissues including the pronephric duct (arrowhead). **z,** 24 hpf. Blue arrow, forebrain; black arrow, otic vesicle; reduced number of *lnx-l* positive neuronal cells (asterisks). From 24 hpf onward, only the posterior dorsal aorta expresses *lnx-l* (blue arrowhead). Black arrowhead, pronephric duct. **a'-c',** 48 hpf. **a',** black arrow, otic vesicle; blue arrowhead pronephric duct; black arrowhead, pharyngeal arch; blue arrow, liver. **b',** Arrowheads indicate pharyngeal arches. **c',** Black arrow, otic vesicle; blue arrow, liver; arrowhead, pronephric duct. **A,** Transverse section of sphere stage embryo (**b,** line A); *lnx-l* is expressed in yolk syncytial layer (arrow). **B**, Anterior transverse section, and **C**, posterior transverse section of the embryo in **x**. Arrow, a neuronal cell; blue arrowhead, anterior dorsal aorta, black arrowhead, pronephros. **C**, arrow, ventral ICM where *lnx-l* is expressed transiently; blue arrowhead, dorsal aorta; black arrowhead, pronephric duct. **D,** Transverse section of *cloche* mutant in **y**; *lnx-l*

transcripts are absent from the dorsal aorta and ICM, but present in the pronephric duct (arrowheads). **E,** Transverse section of embryo in **z**. Blue arrowhead, posterior dorsal aorta; black arrowheads, pronephric duct; *lnx-l* is not expressed in ICM at 24 hpf. Abbreviations: CN, central nerve; ICM, intermediate cell mass; NT, notochord; YSL, yolk syncytial layer. Scale bars, 200 μm (in **a, a'** for **a-a'**). **d',** Developmental expression of three zebrafish *lnx* genes analyzed by RT–PCR. Cycle numbers are shown in parenthesis. Primers used:

Lnx-l forward; 5'-CTGGATTGGAAATATTTGGTTGCTTCTCATC-3'

Lnx-l reverse; 5'-TGTTGTGCAGATGAGGTTGCAACTCACAACG-3'

Lnx-1 forward; 5'-GGAAAACATTTCATCCTACGACACCATATC-3'

Lnx-1 reverse; 5'-GAGAGTCCATAGTGTGACGCTCCTTTACAC-3'

Lnx-2 forward; 5'-GTGCACACAGGCTCCACCTTGACCAGG-3'

Lnx-2 reverse; 5'-GATGGCGACCAGCTTGCATCGTAGTCATTTTC-3'

Boz forward; 5'-ATGGCAACTCAGAAGTTTTCAAACTTCTCC-3'

Boz reverse; 5'-CTAATCTGATTCCTGATGATCCTCCAGAGC-3'

β-actin forward; 5′-GAGGAGCACCCCGTCCTGCTCAC-3′

β-actin reverse; 5′-GATGGCTGGAACAGGGCCTCTG-3′

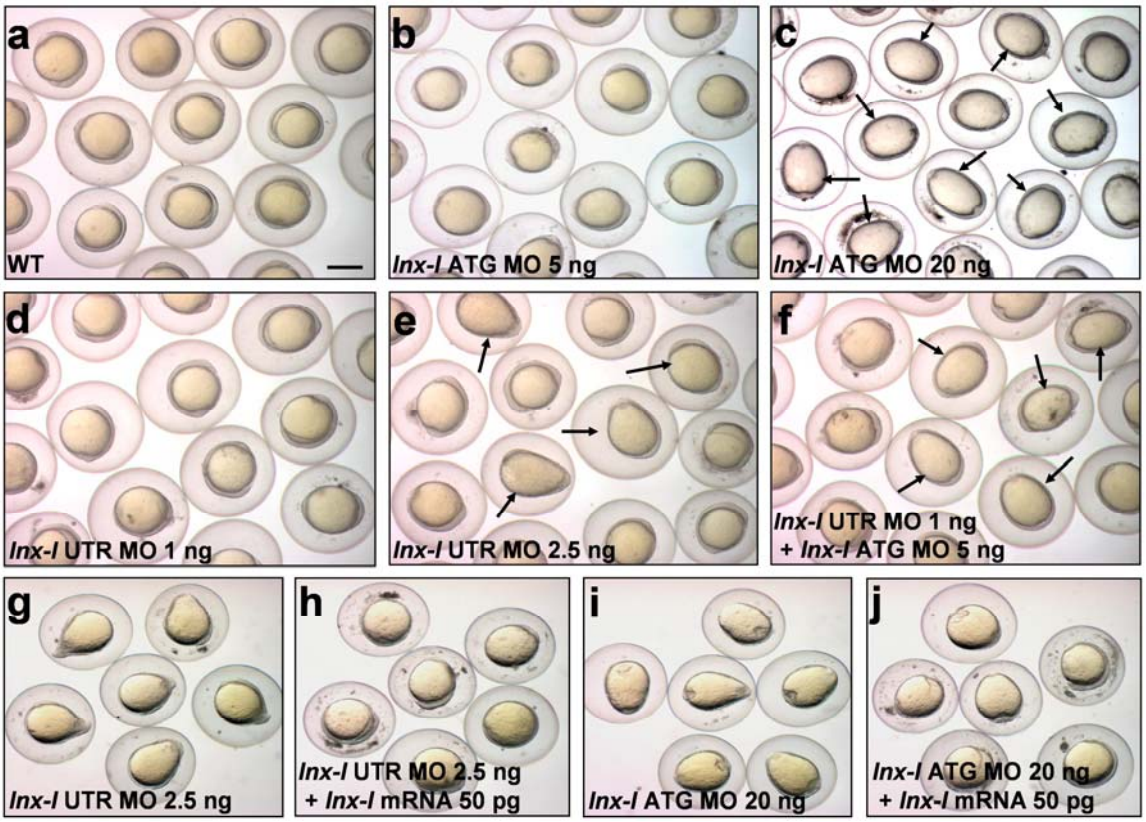

Supplementary Figure 3 | Synergy and rescue of *lnx-l* MOs. a-f, 3-somite stage embryos. **a,** Uninjected. **b,** Low dose of *lnx-l* ATG MO (5 ng) did not induce dorsalization (0% dorsalized, N=80). **c,** High dose of *lnx-l* ATG MO (20 ng) induced dorsalization (76%, N=98). **d,** Low dose of *lnx-l* UTR MO (1 ng) did not induce dorsalization (6%, N=89). **e,** High dose of *lnx-l* UTR MO (2.5 ng) induced dorsalization (64%, N=90). **f,** Embryos were highly dorsalized (arrows) by combined low doses of ATG and UTR MO (69%, N=78). **g-j,** Rescue experiments; all at 3-somite stage. **g,** 2.5 ng *lnx-l* UTR MO-injected embryos showed elongated body axis, characteristic of dorsalization (83% dorsalized, N=72). **h,** The phenotype was relieved by coinjection of 50 pg *lnx-l* mRNA (16% dorsalized, N=90). **i,** 20 ng *lnx-l* ATG MO caused strong dorsalization (81%, N=52). **j,** 50 pg *lnx-l* mRNA rescued the phenotype (40% dorsalized, N=58). To rescue ATG morphants, we mutated four nucleotides in the MO-targeted sequences of *lnx-l* mRNA without affecting the amino acid sequence (GCCATGACGGAGTCT → GaaATGACaGAaTCT). Scale bar, 400 μm.

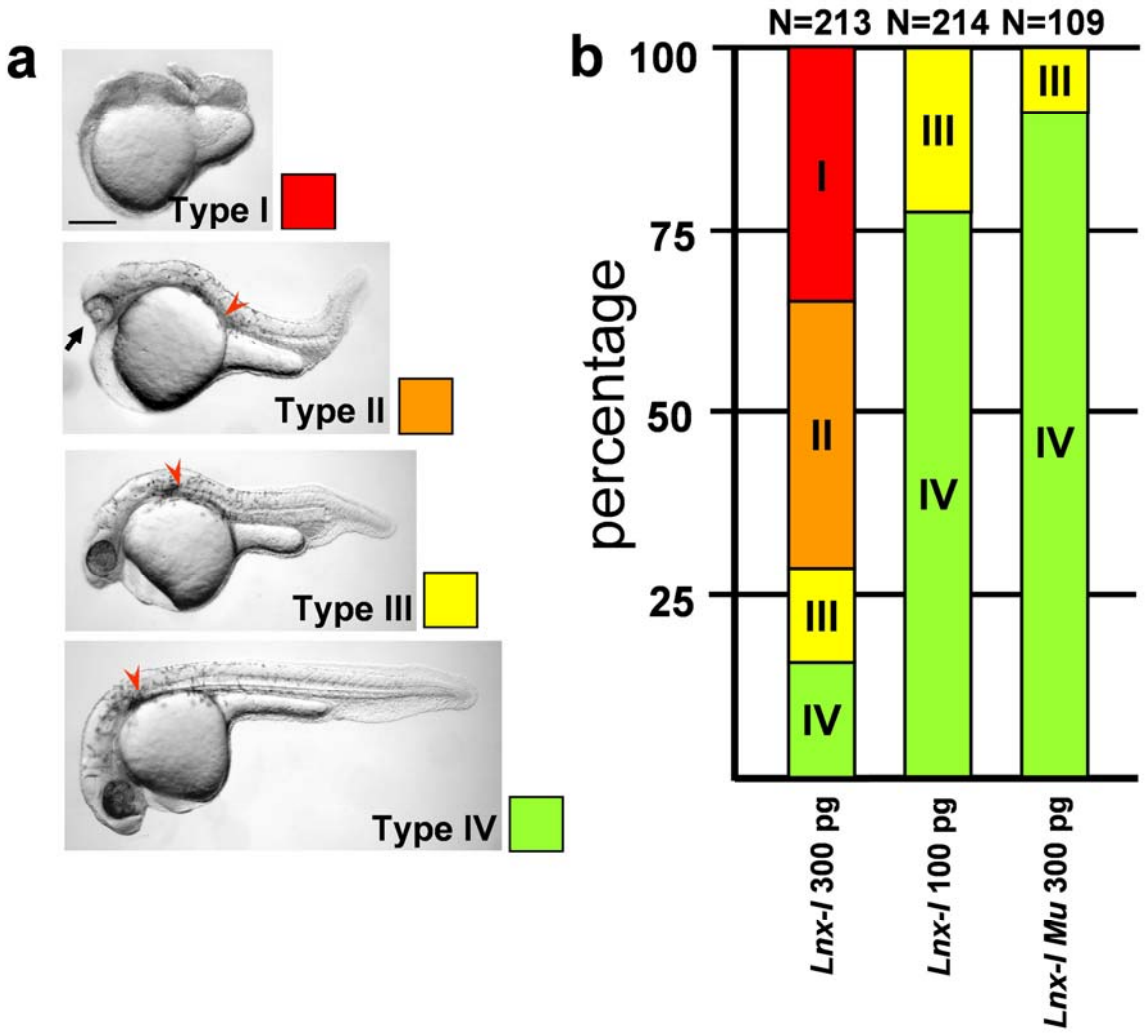

Supplementary Figure 4 | *Lnx-l* overexpression causes axial mesoderm defects. a, Embryonic defects caused by gain-of-function of *lnx-l* were classified into four categories. Type I embryos are most severely defective. Type II embryos showed cyclopia, anterior notochord defects, bent tail and shortened body axis. Type III embryos show anterior notochord defect and shortened body axis. Morphologically unaffected embryos were classified as type IV. Black arrow indicates fused eye. Red arrowheads indicate anterior end point of the notochord. **b,** Summary of embryonic malformations. Total numbers of embryos are shown at the top. Severity of the defect induced by *lnx-l* mRNA was dose dependent; less than 100 pg RNA did not cause observable defects. The axial mesoderm defects observed depend on the E3 ubiquitin ligase activity of Lnx-l as *lnx-l Mu* mRNA encoding a non-functional RING domain did not induce substantial defects even at a high dose. Scale bar, 200 μm.

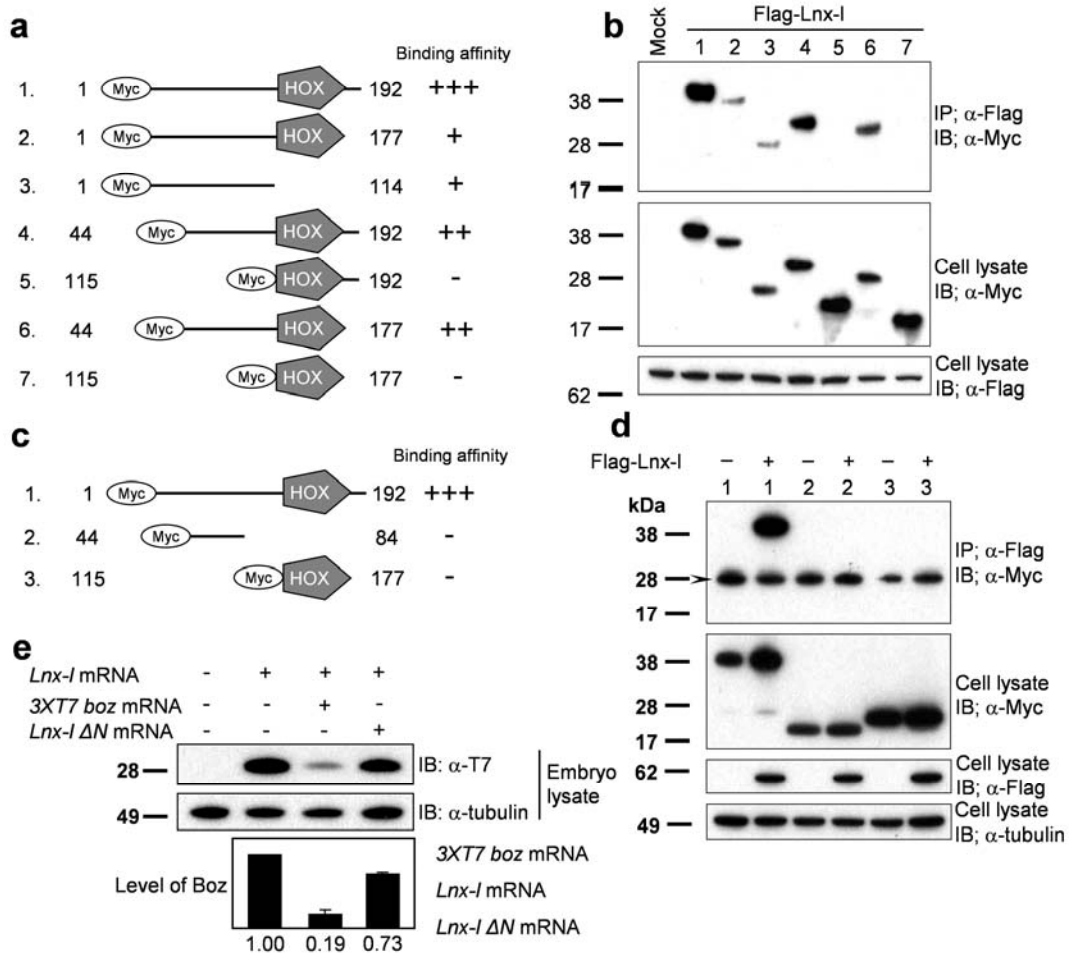

Supplementary Figure 5 | Mapping of Lnx-l binding domains in Boz and Boz destabilization in embryos. a, Schematic diagram of Boz deletion mutants. **b,** To map the binding domains of Boz, we transfected 6xMyc-tagged deletion constructs together with Flag-tagged Lnx-l into the 293T cells. After 48 h, lysates were subjected to IP and IB. Note that the C-terminal region of Boz including the homeodomain (Hox) failed to interact with Lnx-l (lanes 5 and 7). **c,** Schematic diagram of Boz deletion constructs. **d,** The binding assay was carried out as described in **b**. Note that the amino acid 44-84 fragment of Boz did not interact with Lnx-l. Arrowhead in **d**; unidentified background signal. **e,** The RING domain of Lnx-l is critical for the negative regulation of Boz stability**.** 20 pg *3xT7 boz* mRNA was injected into zebrafish embryos with 50 pg *lnx-l* or 50 pg *lnx-l* Δ*N* mRNA. After 6h, the embryos were subjected to IB for 3xT7 Boz. Error bars were obtained from two repeats each of two independent experiments. α-tubulin was used as loading control.

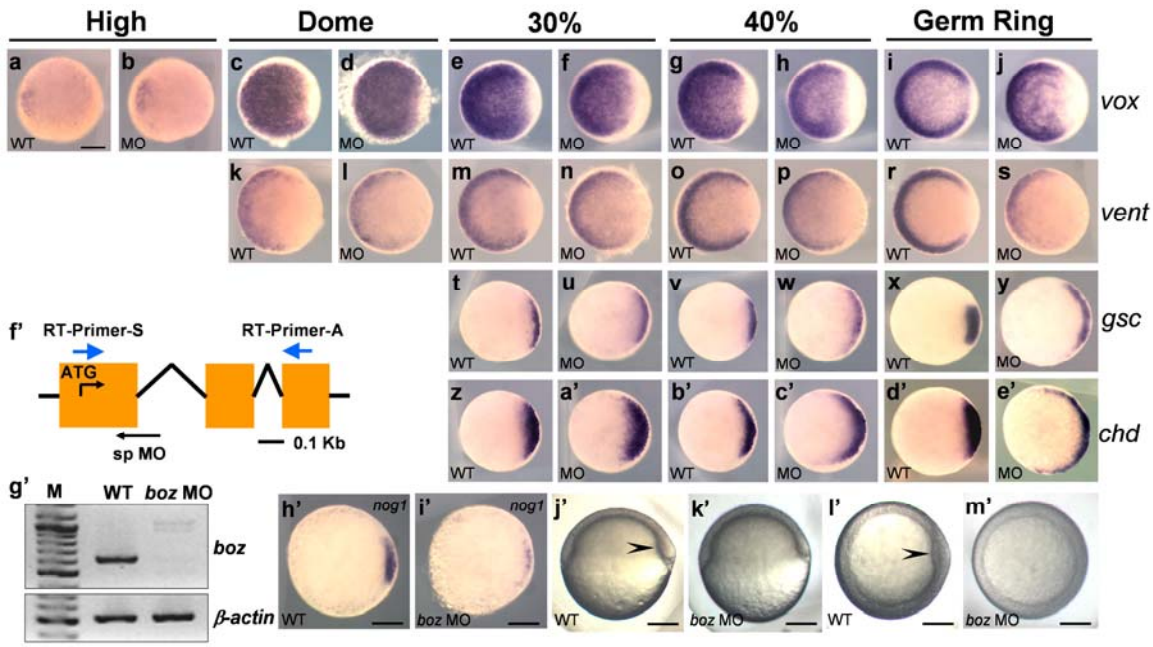

Supplementary Figure 6 | a-e', Lnx-l is involved in maintenance but not initial establishment of the D-V pattern. *gsc* and *chd* are direct targets of Vox and Vent[26,33-35], while *vox* and *vent* are negatively regulated by Boz [25-27]. *Lnx-l* morphants are similar to embryos missing *vox* and *vent* (Df^{st7})[36]. **a-j,** *vox* expression. **k-s,** *vent* expression. **t-y,** *gsc* expression. **z-e',** *chd* expression. Stages are indicated at the top, uninjected (WT) and 2.5 ng *lnx-l* UTR MO-injected (MO) embryos are shown. **a** and **b,** high stage, *lnx-l* morphants showed normal *vox* expression (27/27 embryos). **c** and **d, k** and **l,** dome stage, *vox* (27/27) and *vent* expression (30/30) was unaffected. At 30% epiboly, few embryos showed reduced expression of *vox* (**e** and **f,** 6/64) and *vent* (**m** and **n,** 8/35), *gsc* was unaffected (**t** and **u,** 18/18), *chd* was expanded slightly (**z** and **a',** 4/22). At 40% epiboly *vox* (**g** and **h,** 25/74) and *vent* (**o** and **p,** 20/39) were reduced, while *gsc* (**v** and **w,** 10/24) and *chd* (**b'** and **c',** 15/23) were expanded. At the germ ring stage, *vox* (**i** and **j,** 58/77) and *vent* (**r** and **s,** 32/37) were strongly reduced, while *gsc* (**x** and **y,** 29/33) and *chd* (**d'** and **e',** 39/41) were strongly expanded. Panels **i,j,r,s,x,y,d'** and **e'** are the same as the panels in Figure 1e-l, shown again for ease of comparison. All animal pole views, dorsal to the right. **f'-m',** *Boz* splice (sp) MO efficiency. Since a Boz translation-blocking MO was reported to induce neural degeneration[37], a hallmark of MO toxicity, we designed a sp MO. **f',** Schematic drawing of the *boz* gene. *boz* sp MO targets the splice donor site at the exon 1-intron 1 junction. Primers are shown. **g',** *Boz* sp MO blocked production of *boz*

mRNA. A weak band of presumed unspliced RNA is seen. **h', l',** *nog1* expression at germ ring of uninjected embryos (**h'**), and *boz* morphants (**l'**); the reduction of *nog1* phenocopies *boz* mutants[30]. **j'-m',** Shield stage (6 hpf); arrowhead indicates embryonic shield. In *boz* morphants, no shield is visible (**k', m'**). **j', k',** Lateral views; **l', m',** Animal pole views. Scale bar, 200 μm.

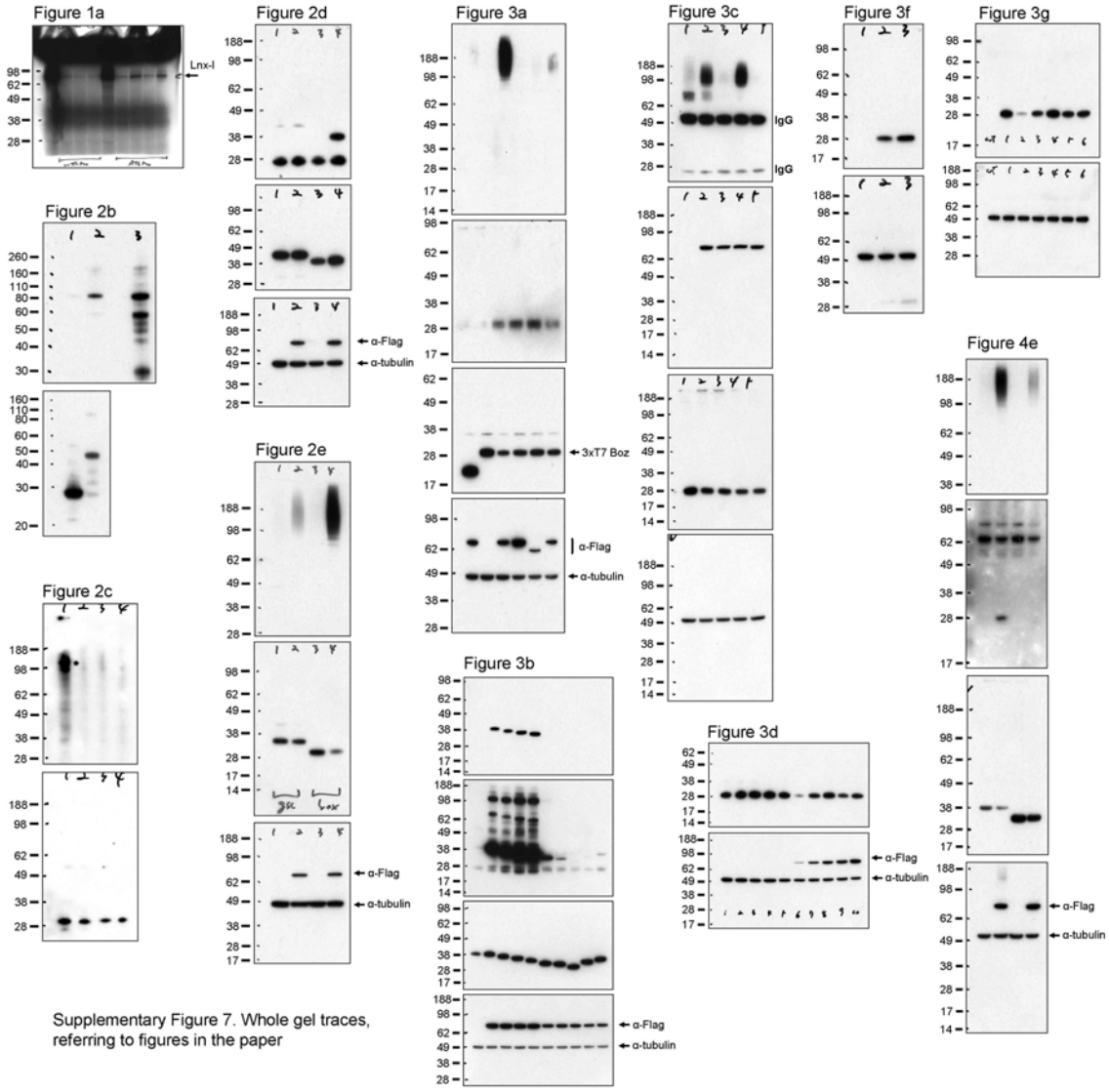

Supplementary Figure 7 | Whole gel traces, referring to figures in the paper.

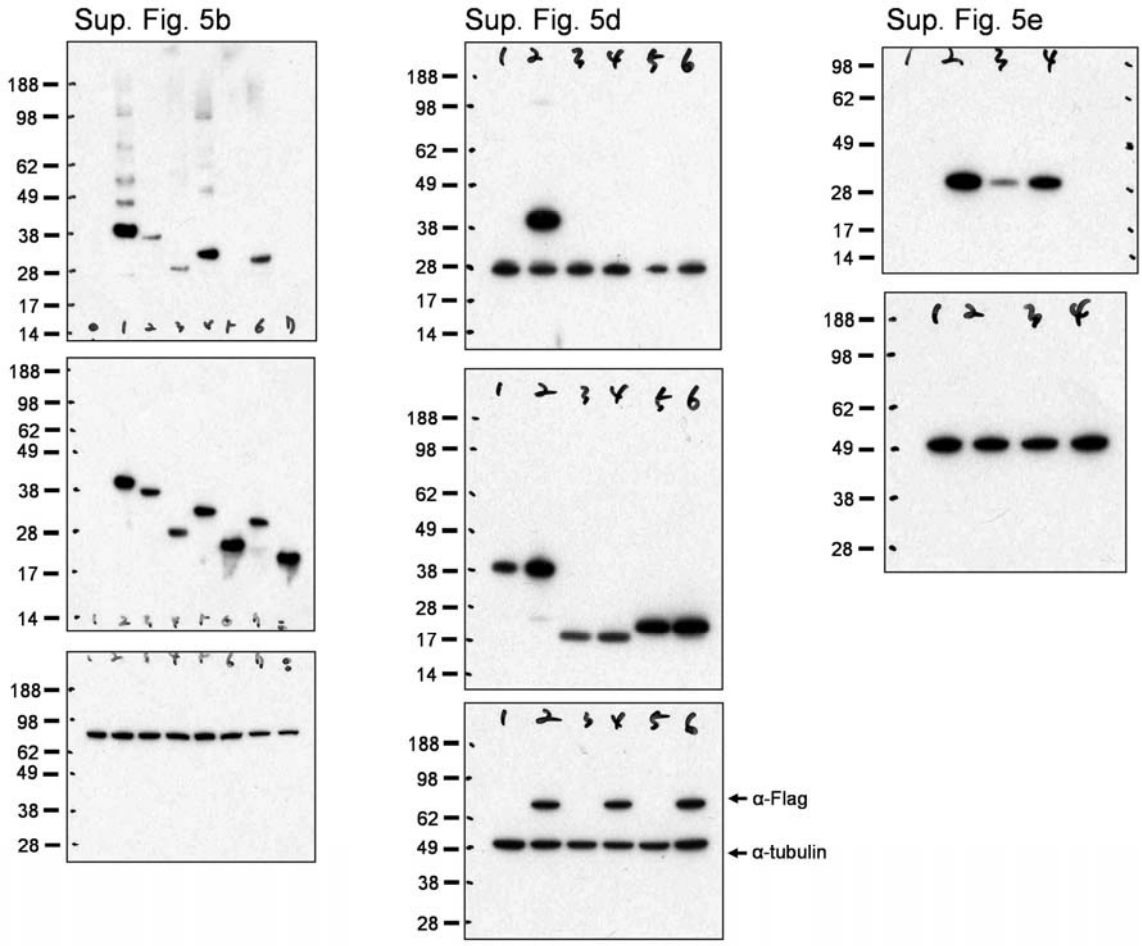

Not for publication – editorial inspection only; Whole gel traces, referring to figures in the supplementary data